Journal of Superconductivity and Novel Magnetism (2021) 34:2523–2530
https://doi.org/10.1007/s10948-021-05934-7

ORIGINAL PAPER

The Role of Buffer Layer on the Performance and Uniformity Improvement of Long-Length HTS $YBa_2Cu_3O_{7-x}$ Tapes Derived by MOD

Chen Liao[1] · Chuanbing Cai[1,2] · Feng Fan[1,2] · Yangyang Chen[1] · Zhiyong Liu[1,2] · Chuanyi Bai[1,2] · Yuming Lu[1,2] · Yanqun Guo[1,2] · Hongbin Jian[2] · Yongjun Zhang[2]

Received: 5 March 2021 / Accepted: 4 June 2021 / Published online: 18 June 2021

Abstract
The present work reports our efforts to enhance the performance and uniformity for the long tapes of metal–organic deposition $YBa_2Cu_3O_{7-x}$ (MOD-YBCO) layer on ion-beam-assisted deposition MgO (IBAD-MgO) template. Reflection High-energy electron diffraction (RHEED) is employed to realize the in-situ growth monitor of IBAD-MgO, as well as the correlation between the quantitative RHEED peaks and in-plane texture of Epi-MgO identified by XRD, which is an effective guide to improve the uniformity and performance of long YBCO tapes. In addition, the surface of the LMO layer during the magnetron sputtering process is improved via controlling the O_2 flux, and then the critical-current density (J_c) of YBCO films has been improved. By optimizing the texture of the MgO layer and precisely controlling the LMO layer growth conditions, the performance and uniformity of YBCO-coated conductors grown by metal–organic deposition (MOD) have been greatly enhanced. The superconducting current-carrying capacities of 12-mm-wide tapes have upgraded steadily from 400–500 A to 500–550 A in past 3 years. The laminated CC tapes with current-carrying capacities of 150–170 A per 4-mm width show good uniformity and high quality along 500-m length, implying being promising for various commercial power applications.

Keywords Metallic-organic deposition · Coated conductors · Performance and uniformity · Texture characterization

1 Introduction

Since the discovery of $LaBa_2Cu_3O_7$ superconductor in the 1980s, the practical wires or tapes with copper oxide high-temperature superconductors have aroused great interest all over the world [1, 2]. The second-generation high-temperature superconducting tapes (2G-HTS) are potential for magnet and power applications because of their high-density current-carrying capacity under high magnetic field and liquid nitrogen temperature [3, 4]. In recent years, more and more institutions and power companies are using high-temperature superconductors for electric power applications such as high-field magnets [5, 6], high-energy physics particle accelerators [7, 8], fusion reactors [9, 10], transmission cables [11, 12], inductive heater [13, 14], and wind turbine [15, 16]. To obtain high performance of 2G-HTS, it is vital to overcome the weak-link of grain boundaries. Several techniques have been developed well to obtain biaxial texture oxide buffer layers on the metal substrates, including ion-beam-assisted deposition (IBAD) [17], inclined-substrate deposition (ISD) [18], and rolling-assisted biaxially textured substrate (RABiTS) [19]. Buffer layers have multiple roles in the architecture, including improving the grain boundaries weak-link, transferring texture to the superconducting layer, and blocking metal atom diffusion from the substrate into the superconducting layer.

Various industrialization routes on 2G-HTS coated conductors have been carried out around the world [20, 21]. After more than 20 years of research and development, multiple technologies such as pulsed laser deposition (PLD), metal–organic chemical vapor deposition (MOCVD), reaction co-evaporation (RCE), and metal–organic deposition

✉ Chuanbing Cai
cbcai@t.shu.edu.cn

✉ Feng Fan
feng_fan@shu.edu.cn

Chen Liao
liaochen@shu.edu.cn

[1] Physics Department, Shanghai Key Laboratory of High Temperature Superconductors, Shanghai University, Shanghai 200444, China

[2] Shanghai Creative Superconductor Technologies Company Ltd, Shanghai 201400, China

(MOD) have been developed for the industrial production of coated conductors, of which the MOD technique is very attractive due to low cost and high yield potential [22–28].

In the present work, we will introduce our efforts to enhance the performance and uniformity of long-length MOD-YBCO tapes by controlling the in-plane texture and surface quality of buffer layers and using continuous characterization tools.

2 Experiment Details

2.1 IBAD-MgO-Based Buffers and Applicable Techniques

The typical architectures of 2G-HTS tape are based on IBAD and MOD techniques. The IBAD-based buffer in the presently coated conductors are stacked as Al_2O_3/Y_2O_3/IBAD-MgO/Epi-MgO/LMO, where the Hastelloy-C276 alloy with excellent mechanical properties and strong corrosion resistance is selected as the metal substrate, and Al_2O_3 is to applied to prevent element diffusing from the metal substrate. IBAD-MgO layer is the initial biaxial texture, and Epi-MgO is designed to repair defects caused by ion bombardment and further improve the biaxial texture, and finally LMO layer is used to reduce the lattice mismatch between MgO and YBCO. In the present work, Y_2O_3 and Al_2O_3 were prepared by ion-beam or electron-beam evaporation on electrochemical polished Hastelloy metal (C276) substrate. The IBAD-MgO and Epi-MgO are deposited in a dual-chamber e-beam evaporation system. The former, i.e., IBAD-MgO, was evaporated by electron-beam and argon ions were generated and accelerated to 800 eV in RF linear sources. Two linear RF sources with a maximum total current of 350 mA were used to assist deposition. The incidence angle of assisting ion beam is 45° relative to the normal substrate. Then, Epi-MgO was grown on IBAD-MgO in the Epi chamber, Epi-MgO is deposited by electron beam evaporation in a vacuum of 4.0×10^{-5} Torr, the deposition rate was 8.0 Å/s, and the O_2 flux rate is 6 SCCM, and the substrate temperature was heated to 650 °C by multi-zone heating. Finally, the $LaMnO_3$ film is deposited on the IBAD-MgO/Epi-MgO template by DC reactive magnetron sputtering.

For the LMO layer, La-Mn alloy with an atomic number ratio of 1:1 and a purity of more than 99.95% was used as a sputtering target. The LMO films with a thickness of about 30 nm were deposited on the MgO template by reactive magnetron sputtering. In order to successfully implement DC reactive sputtering, an active voltage control system was used to monitor the sputtering states and automatically adjust the oxygen flow rate. Typical sputtering conditions include 1-Pa total pressure, Ar/O_2 sputtering gas mixture, and 1000-W power. For the Ar/O_2 mixture, the Ar flow rate was set to 135 SCCM, and the automatic matching O_2 flow rate range was 14.9 to 15.6 SCCM, depending on the set voltage. LMO is deposited at a temperature range of 720–780 °C, which is suitable for the process window.

2.2 Ex-Situ MOD Growth of YBCO Layers

For the synthesis of YBCO precursor solution, barium acetate was dissolved in trifluoroacetic acid diluted by deionized water, and a stoichiometric ratio of Y and Cu acetates were dissolved in propionic acid and deionized water. First, the Y and Cu acetates were put into a constant temperature water bath at 40 °C and stirred for 1 h, and then Ba acetate was put on a magnetic stirrer stir for 40 min until completely dissolved. The above solutions were refined separately by drying and dissolving in methanol. By mixing the two solutions, the precursor solution was obtained. After refining

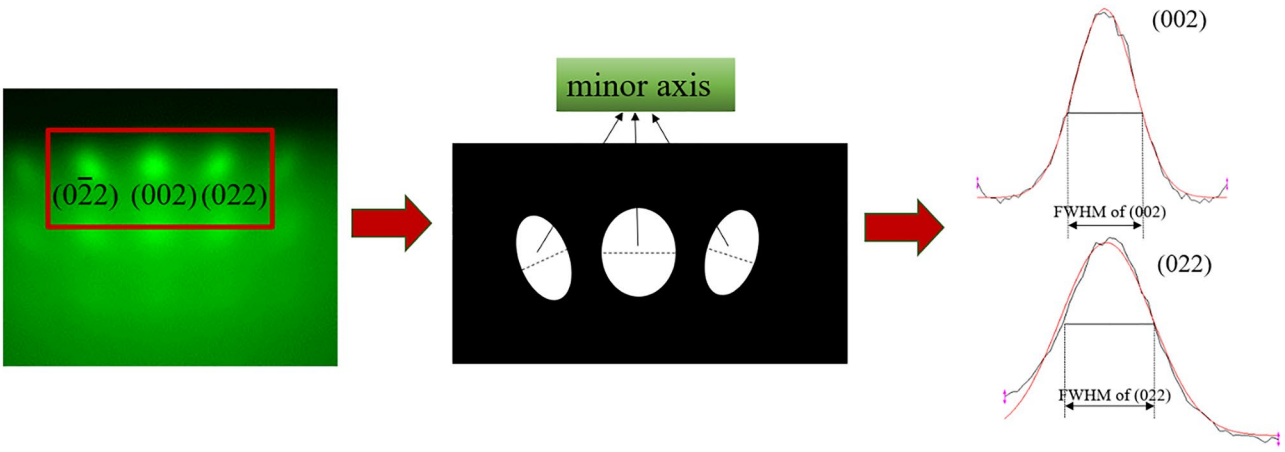

Fig. 1 Analyzing of RHEED spot (002) and (022) for brightness and characteristics. The FWHM was obtained by fitting the minor axis data of the black-and-white spots, and the relative value of (002) and (022) FWHM was defined as the ratio

the mixed Y, Ba, and Cu solutions for several times, methanol was added again to get the desired concentration, i.e., 2.5 mol/L, the molar concentration of the metal ions in the final precursor solution. More details of the YBCO deposition can be found elsewhere [29, 30].

2.3 Texture and Critical Current Characterization

X-ray diffraction (XRD) was used to measure the crystal structure and texture of short samples. The out-of-plane texture of Epi-MgO for the long tapes were determined by a home-made reel-to-reel XRD diffractometer. Reflection high-energy electron diffraction (RHEED) was employed to qualitatively monitor the epitaxial growth of IBAD-MgO as well as Epi-MgO. The surface roughness was characterized by atomic force microscope in contact mode.

The inductive critical current density, J_c (77 K, self-field), for the short-length samples were measured using the Cryoscan made by THEVA. The continuous measurement for critical current I_c (77 K, self-field) was carried out by both inductive and transport tools, a Tapestar™ XL made by THEVA, and a home-made reel-to-reel four-probe system, respectively.

3 Result and Discussion

According to our experiment, the brightness and shape of the RHEED MgO (002) and (022) spots are significant parameters among all spots. Therefore, a quantitative analysis method for RHEED is deduced to help us to comprehend the texture of IBAD-MgO in real time. The analysis process is shown in Fig. 1. First, the data along the short axis of (002) and (022) spots are extracted from the IBAD-MgO image taken by KSA 400 software. The FWHM values were obtained through data fitting, giving rise to a relative value of (002) FWHM to (022) FWHM (hereinafter referred to as ratio) which was then compared with the similar characterization based on ex-situ XRD measurement.

Figure 2 shows the RHEED patterns for short samples of IBAD-MgO at various deposition rates, such as 8.0 Å/s, 8.6 Å/s, and 9.2 Å/s. At the deposition rate of 8.0 Å/s, the RHEED patterns of IBAD-MgO show dispersal with only low-index diffraction spots present, implying that the process involves a higher ion-to-molecule ratio and then the films are over etched. At a relatively high deposition rate, diffraction spots become brighter. As the deposition rate increases to be 8.6 and 9.2 Å/s, a clear RHEED pattern occurs with sharp diffraction spots, indicating that the out-of-plane texture are achieved better.

Further, the in-plane texture of subsequent Epi-MgO is characterized by the XRD phi-scan. The relationship between the FWHM of MgO (220) phi-scan and the deposition rate of IBAD-MgO are studied for the case of assisting E-beam current fixed at 202 mA. As shown in Fig. 3, as the deposition rate is 8.0 Å/s, the FWHM of MgO (220) phi-scan exhibits a large value suggesting that the in-plane texture is bad. With the increase of the deposition rate, the in-plane texture of MgO is improved much better at the deposition rate ranges from 8.2 Å/s to 9.0 Å/s. As the deposition rate increases further, in-plane texture of MgO begins to deteriorate again. The results show that under the beam current of 202 mA, MgO with good in-plane texture can be obtained within a suitable deposition rate range. Note that, compared with XRD, RHEED pattern is hard to

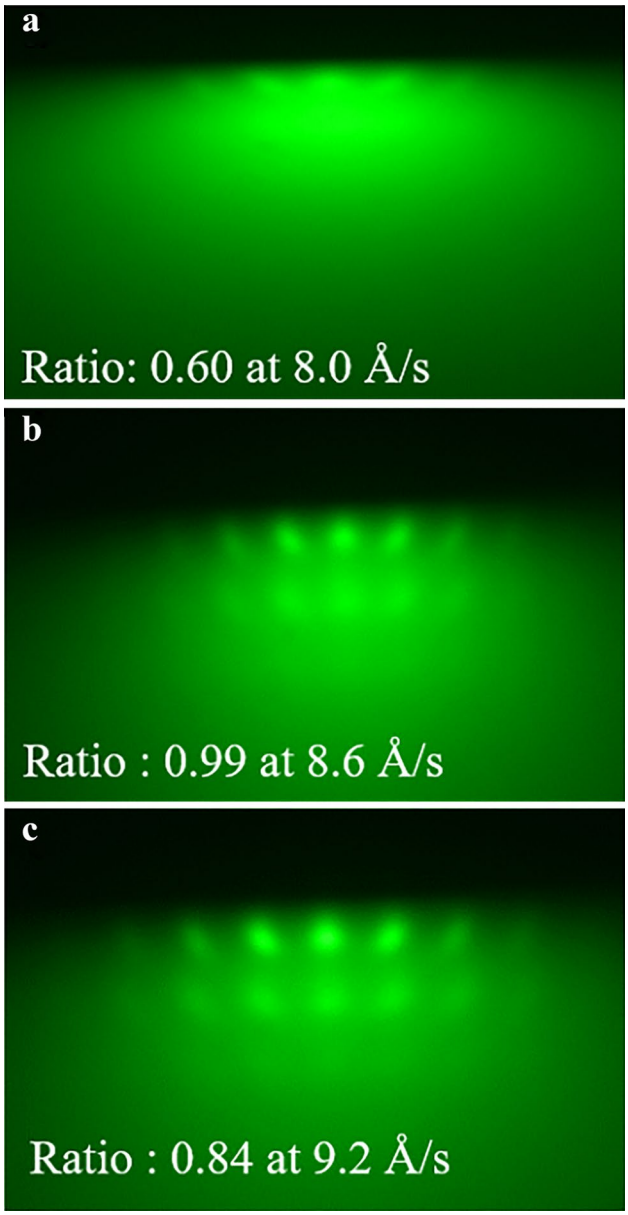

Fig. 2 RHEED patterns for short samples of IBAD-MgO at deposition rates at 8.0 Å/s, 8.6 Å/s, and 9.2 Å/s

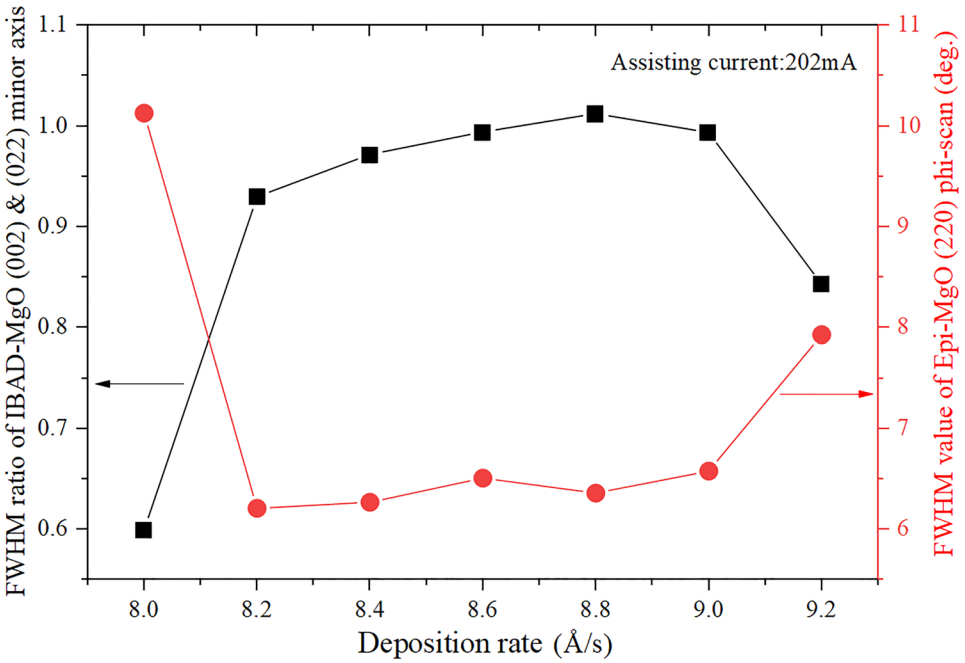

Fig. 3 Correlation between the intensity of RHEED spots and FWHM value of MgO (220) phi-scan results was assessed at different deposition rates from 8.0 Å/s to 9.2 Å/s under the current of 202 mA

quantitatively monitor the slight degradation of in-plane texture for Epi-MgO.

In order to achieve quantitative characterization of in-plane texture using RHEED of IBAD-MgO, the correlation between the ratio of IBAD-MgO (002) and (022) minor axis and FWHM value of MgO (220) XRD phi-scan are studied. As in Fig. 3, it can be seen that the ratio shows the same trend as the FWHM of Epi-MgO (022) phi-scan by XRD. The results indicate that relying on the ratio of RHEED can be a reliable and real-time method to observe the quality of MgO. As the strength is in the range of 0.9 to 1.1, the good biaxial texture of MgO layer can be obtained.

In addition to significant improvement on the IBAD and RHEED process, the roughness of subsequent LMO is optimized by adjusting the temperature in the reactive sputtering to enhance the superconducting performance of YBCO.

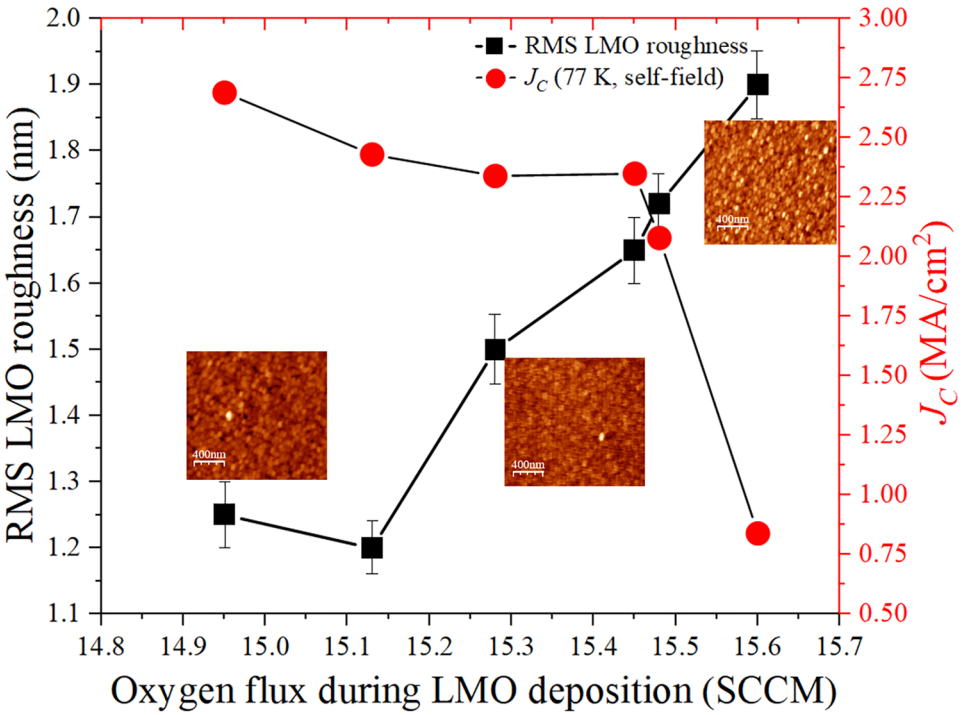

Fig. 4 Oxygen flux during LMO deposition versus RMS LMO surface roughness, and J_c of YBCO deposited by MOD on the LMO substrate. The oxygen flux affects the roughness of the LMO surface, which in turn affects the J_c of YBCO. When the LMO roughness increases to the critical value, J_c suddenly decreases (illustration: AFM images of LMO under O_2 flux of 14.9 SCCM, 15.28 SCCM, and 15.6 SCCM)

However, oxygen flow in the reactive sputtering is more likely to affect surface roughness. As a result, it is found that the surface roughness of LMO strongly depends on the oxygen flow rate, and the relationship that the oxygen flux rate affects the LMO roughness surface and then affect the J_c of YBCO indeed exists and is repeatable. We have done many batches and combined with experimental data, found that they all have such regular. What is mentioned in the paper is a typical data in a large number of statistics. Figure 4 shows the relationship between RMS surface roughness of LMO, J_c, and oxygen flow, respectively. It is seen that with the increase oxygen flow, the RMS value increases monotonously from 1.25 nm to 2.3 nm. As the oxygen flows faster, J_c value decreases monotonously from 2.7 MA/cm^2 to 0.7 MA/cm^2, respectively. Note that as the oxygen flow rate increases to a critical value, the value of J_C drops much. This trend is mainly attributed to rapid growth in case of high oxygen flow, resulting in the increase in surface roughness, and thus the drop in J_c; i.e., as the surface flatness of LMO improves, the J_c is enhanced by controlling the oxygen flow during LMO growth.

Furthermore, the relationship between MgO (002) XRD omega-scan and final I_c (77 K, self-field) is summarized in Fig. 5. It is obvious that the I_c of YBCO films is closely relevant to the FWHM of MgO (002). As the FWHM of ω-scan increases, the I_c decreases accordingly, which allows us be able to predict the I_c based on the FWHM of ω-scan, and thereby guides us to improve the growth process of IBAD-MgO/Epi-MgO.

Figure 6 shows that recent improvement on the performance of YBCO coated conductor is achieved in Shanghai Creative Superconductor Technologies Company SCSC. As shown in Fig. 6a, the superconducting current-carrying capacity of 12-mm-wide tapes has increased from 400–500 A to 500–550 A in the past 3 years. After slitting and laminating, the 4-mm-wide tapes with current-carrying capacity of 150–170 A are typically obtained, as presented in Fig. 6b. Along the tape length of more than 500 m, an excellent uniformity of long tape performance is realized, implying

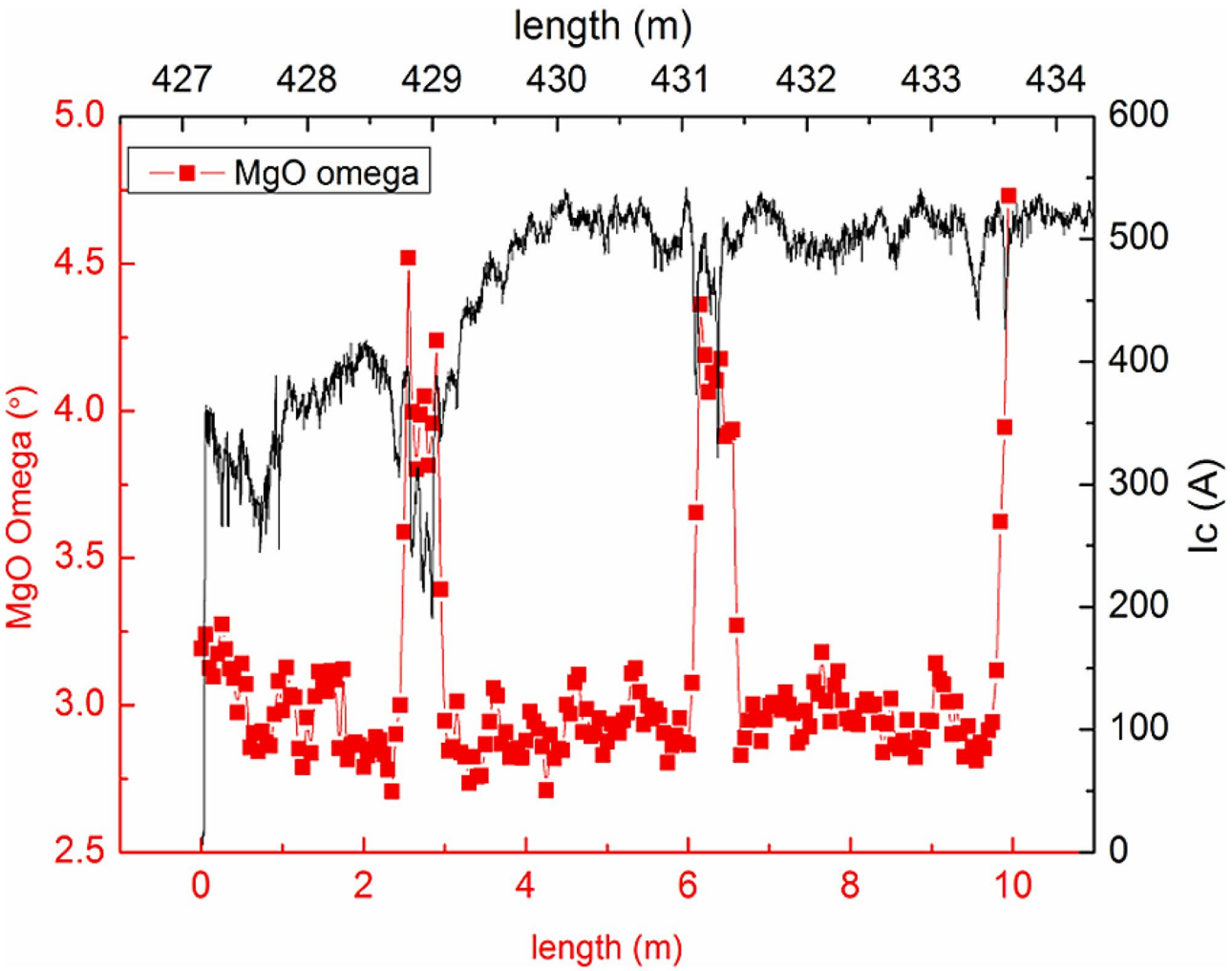

Fig. 5 The relationship between MgO (002) omega-scan tapes and I_c of YBCO tapes (77 K, self-field)

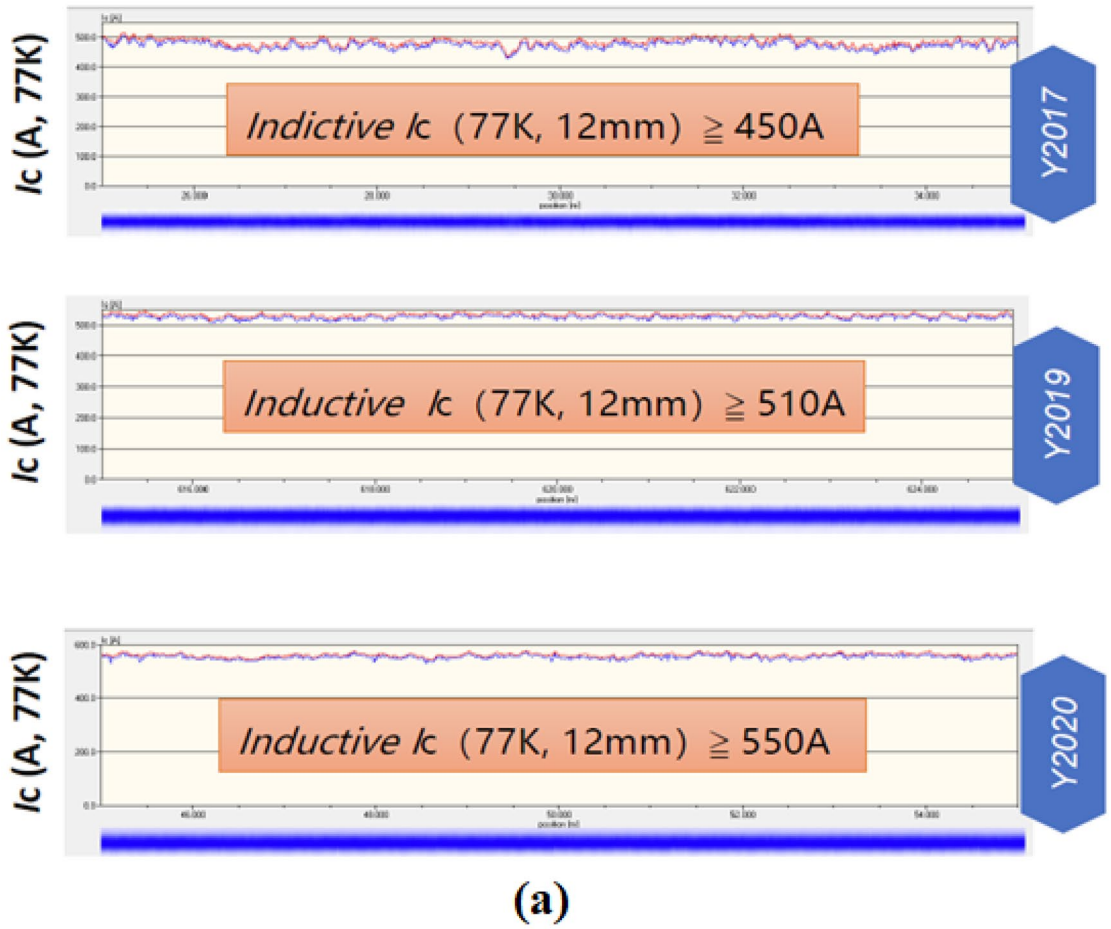

(a)

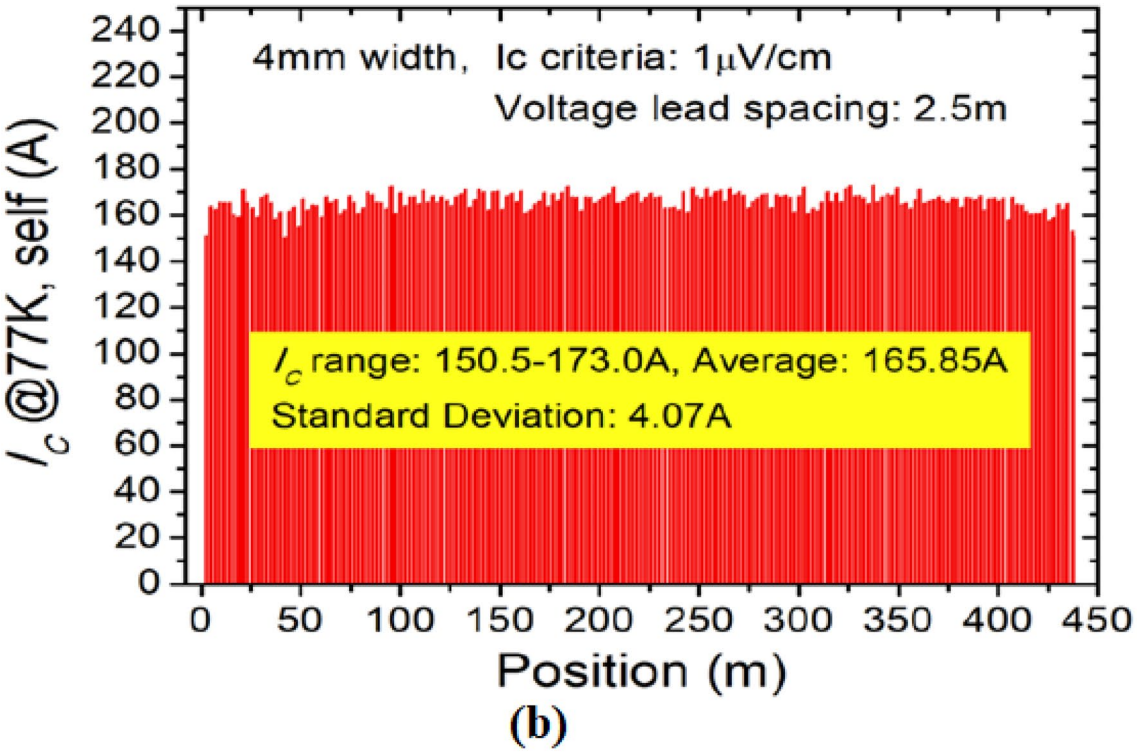

(b)

Fig. 6 I_c distribution along the tapes with various widths: **a** 12 mm wide, 50 m long in 2017, 2019, and 2020 and **b** 4 mm wide, 500 m long with brass laminations

that the present long 2G-HTS tapes satisfy the commercial requirements for various power applications.

4 Conclusions

In summary, the relationship between a relative value of IBAD-MgO (002) FWHM to (022) FWHM and Epi-MgO (220) in-plane texture was established, which could achieve the quantitative characterization and monitoring of the IBAD-MgO texture growth. As well, the I_c drop points in long-length YBCO tapes could be found out effectively by reel-to-reel XRD measurement system, which is helpful for evaluating the stability of YBCO tapes. The current-carrying capacity of the YBCO film exhibited a strong dependence on the surface of the LMO film. By adjusting the O_2 flux to optimize the surface flatness of the LMO, the current-carrying capacity of the YBCO coated conductor was improved. In the past few years, the superconducting current-carrying capacity for 12-mm-wide tape has steadily increased from 400 A to more than 550 A. The laminated CCs tape for 4-mm-wide tape exhibits high critical current and good uniformity over than 500-m-long tape, being qualified for various commercial power applications.

Funding This work was supported in part by the Strategic Priority Research Program of Chinese Academy of Sciences (XDB25000000), the National Key Research and Development Program (2016YFF0101701), and the Field Foundation of Pre-Research on Equipment under Grant (6140923050202).

References

1. Bednorz, J.G., Müller, K.A.: Possible high T_c superconductivity in the Ba-La-Cu-O system. Zeitschrift Für Phys. B Condens. Matter. **64**, 189–193 (1986). https://doi.org/10.1007/BF01303701
2. Bondarenko, S.I., Koverya, V.P., Krevsun, A.V., Link, S.I.: High-temperature superconductors of the family (RE)$Ba_2Cu_3O_{7-\delta}$ and their application (Review Article). Low Temp. Phys. **43**, 1125–1151 (2017). https://doi.org/10.1063/1.5008405
3. Fietz, W.H., Barth, C., Drotziger, S., Goldacker, W., Heller, R., Schlachter, S.I., Weiss, K.: Prospects of high temperature superconductors for fusion magnets and power applications. Fusion Eng. Des. **88**, 440–445 (2013). https://doi.org/10.1016/j.fusengdes.2013.03.059
4. van der Laan, D.C., Goodrich, L.F., Haugan, T.J.: High-current dc power transmission in flexible $REBa_2Cu_3O_{7-\delta}$ coated conductor cables. Supercond. Sci. Technol. **25**, 014003 (2012). https://doi.org/10.1088/0953-2048/25/1/014003
5. Hahn, S., Kim K., Kim, K., Hu, X., Painter, T., Dixon, I., Kim, S., Bhattarai, K.R., Noguchi, S., Jaroszynski, J., Larbalestier, D.C.: 45.5-tesla direct-current magnetic field generated with a high-temperature superconducting magnet, Nature. **570,** 496–499 (2019) . https://doi.org/10.1038/s41586-019-1293-1
6. Awaji, S., Imai, Y., Takahashi, K., Okada, T., Badel, A., Miyazaki, H., Hanai, S., Ioka, S.: Field stability analysis of 25 T cryogen-free superconducting magnet and upgrade plans for 30 T system at HFLSM, IMR, Tohoku University. IEEE Trans. Appl. Supercond. **29**, 1–5 (2019). https://doi.org/10.1109/TASC.2019.2898699
7. Ballarino, A.: High temperature superconducting current leads for the large hadron collider. IEEE Trans. Appiled Supercond. **9**, 523–526 (1999). https://doi.org/10.1109/77.783350
8. Wilson, M.N.: Superconductivity and accelerators: the good companions. IEEE Trans. Appiled Supercond. **9**, 111–121 (1999). https://doi.org/10.1109/77.783250
9. Bruzzone, P., Sedlak, K., Uglietti, D., Bykovsky, N., Muzzi, L., Marzi, G., Celentano, G., Corte, A.: Si Turtù, M Seri, LTS and HTS high current conductor development for DEMO. Fusion Eng. Des. **96**, 77–82 (2015). https://doi.org/10.1016/j.fusengdes.2015.06.150
10. Heller, R., Fietz, W.H., Kienzler, A., Lietzow, R.: High temperature superconductor current leads for fusion machines. Fusion Eng. Des. **86**, 1422–1426 (2011). https://doi.org/10.1016/j.fusengdes.2010.12.077
11. Yang, P., Wang, Y., Qiu, D., Chang, T., Ma, H., Zhu, J., Jin, Z., Hong, Z.: Design and Fabrication of a 1-MW High-temperature superconductor DC induction heater. IEEE Trans. Appl. Supercond. **28**, 1–5 (2018). https://doi.org/10.1109/TASC.2018.2810498
12. Choi, J., Kim, S.K., Kim, S., Sim, K., Park, M., Yu, I.K.: Characteristic analysis of a sample HTS magnet for design of a 300 kW HTS DC induction furnace. IEEE Trans. Appl. Supercond. **26**, 1–5 (2016). https://doi.org/10.1109/TASC.2016.2524686
13. Song, X., Mijatovic, N., Kellers, J., Buhrer, C., Rebsdorf, A.V., Hansen, J., Christensen, M., Krause, J., Wiezoreck, J., Putz, H., Holboll, J.: A full-size high-temperature superconducting coil employed in a wind turbine generator setup. IEEE Trans. Appl. Supercond. **27**, 1–5 (2017). https://doi.org/10.1109/TASC.2017.2656627
14. Song, X., Bergen, A., Winkler, T., Wessel, S., Ter Brake, M., Kellers, J., Putz, H., Bauer, M., Kyling, H., Boy, H., Seitz, E., Buhrer, C., Brutsaert, P., Krause, J., Ammar, A., Wiezoreck, J., Hansen, J., Rebsdorf, A.V., Dhalle, M.: Designing and basic experimental validation of the world's first MW-class direct-drive superconducting wind turbine generator. IEEE Trans. Energy Convers. **34**(2), 218–2225 (2019). https://doi.org/10.1109/TEC.2019.2927307
15. van der Laan, D.C., Lu, X.F., Goodrich, L.F.: Compact $GdBa_2Cu_3O_{7-\delta}$ coated conductor cables for electric power transmission and magnet applications. Supercond. Sci. Technol. **24**, 042001 (2011). https://doi.org/10.1088/0953-2048/24/4/042001
16. Na, J.B., Sung, H.G., Choi, C.Y., Jang, Y., Hun, Y.: Design of 23kV 50MVA class HTS cable in South Korea. J. Phys. Conf. Ser. **1054**, 012073 (2018). https://doi.org/10.1088/1742-6596/1054/1/012073
17. Iijima, Y., Matsumoto, K.: High-temperature-superconductor coated conductors: technical progress in Japan. Supercond. Sci. Technol. **13**, 68–81 (2000). https://doi.org/10.1088/0953-2048/13/1/310
18. Prusseit, W., Sigl, G., Nemetschek, R., Hoffmann, C., Handke, J., Lumkemann, A., Kinder, H.: Commercial coated conductor fabrication based on inclined substrate deposition. IEEE Trans. Appiled Supercond. **15**, 2608–2610 (2005). https://doi.org/10.1109/TASC.2005.847680
19. Goyal, A., Paranthaman, M.P., Schoop, U.: The RABiTS approach: using rolling-assisted biaxially textured substrates for high-performance YBCO superconductors. MRS Bull. **29**, 552–561 (2004). https://doi.org/10.1557/mrs2004.161
20. Zhao, Y., Zhu, J., Jiang, G. et al. Progress of second-generation high temperature superconducting tape fabrication at Shanghai superconductor technology, Supercond. Sci. Technol. **32**(4) 2019. https://doi.org/10.1088/1361-6668/aafea5
21. Vlad, V.R., Usoskin, A., Lee, S., Petrykin, V., Molodyk, A., Bartolome, E., Vilardell, M., Calleja, A., Meledin, A., Obradors, X., Puig, T., Ricart, S., Van Tendeloo, G.: Inkjet printing multi-deposited YBCO on CGO/LMO/MgO/Y_2O_3/Al_2O_3/Hastelloy tape for 2G-coated conductors. IEEE Trans. Appl. Supercond. **28**, 1–5 (2018). https://doi.org/10.1109/TASC.2018.2808403

22. Lu, Y.M., Cai, C.B., Liu, Z.Y., Guo, Y.Q., Bin Jiang, H., Zhang, Y.J., Li, M.J., Fan, F., Bai, C.Y., Lu, Q., Dou, W.Z., Yang, W.: Advance in long-length REBCO coated conductors prepared by reel-to-reel metalorganic solution and ion-beam-assisted deposition, IEEE Trans. Appl. Supercond. **29** (2019) 1–5. https://doi.org/10.1109/TASC.2019.2910021
23. Cayado, P., Mundet, B., Obradors, X., et al.: Epitaxial superconducting $GdBa_2Cu_3O_{7-\delta}/Gd_2O_3$ nanocomposite thin films from advanced low-fluorine solutions. Supercond. Sci. Technol. **30**, 125010 (2017). https://doi.org/10.1088/1361-6668/aa8ffe
24. Sathyamurthy, S., Thieme, C., Rupich, M.W.: American superconductor: second generation superconductor wire—from research to power grid applications [J]. Springer International Publishing **224**, 131–165 (2016). https://doi.org/10.1007/978-3-319-23419-9_5
25. Xuming, X., Sungjin, K., Zdun, K. et al. Progress in high throughput processing of long-length, high quality, and low cost IBAD MgO buffer tapes at SuperPower, IEEE Trans. Appl. Supercond. **19** (2009) 3319–3322. https://doi.org/10.1109/TASC.2009.2018816
26. Martynova, I., Tsymbarenko, D., Kamenev, A., Amelichev, V., Molodyk, A., Kuzmina, N., Kual, A.: Solution deposition of ultrasmooth alumina on long-length metallic substrate for 2G superconducting tapes. Mater. Res. Bull. **78**, 64–71 (2016). https://doi.org/10.1016/j.materresbull.2016.02.014
27. Lee, J.-H., Lee, H., Lee, J.-W., Choi, S.-M., Yoo, S.-I., Moon, S.-H.: RCE-DR, a novel process for coated conductor fabrication with high performance. Supercond. Sci. Technol. **27**, 044018 (2014). https://doi.org/10.1088/0953-2048/27/4/044018
28. Usoskin, A., Betz, U., Hofacker, F., Rutt, A., Schlenga, K., Prause, B., Rossi, L., Bottura, L., Ballarino, A., Goldacker, W., Meledin, A., Abraimov, D., Larbalestier, D., Senatore, C., Kario, A.: Double-disordered HTS-coated conductors and their assemblies aimed for ultra-high fields: large area tapes, IEEE Trans. Appl. Supercond. **28** (2018) 1–6. https://doi.org/10.1109/TASC.2018.2801348
29. Cui, C., Liu, Z., Lin, J., Guo, Y., Fan, F., Cai, C.: Thick DyBCO/YBCO multilayer films on $LaMnO_3$ substrate derived by metal organic deposition method. J. Supercond. Nov. Magn. **29**, 1611–1616 (2016). https://doi.org/10.1007/s10948-016-3419-0
30. Li, M., Yang, W., Shu, G., Bai, C., Lu, Y., Guo, Y., Liu, Z., Cai, C.: Controlled-growth of $YBa_2Cu_3O_{7-\delta}$ film using modified low-fluorine chemical solution deposition. IEEE Trans. Appl. Supercond. **25**, 1–4 (2015). https://doi.org/10.1109/TASC.2014.2371534